INTERNATIONAL JOURNAL FOR NUMERICAL METHODS IN BIOMEDICAL ENGINEERING
Int. J. Numer. Meth. Biomed. Engng. 2010; **26**:1219–1227
Published online 26 March 2010 in Wiley Online Library (wileyonlinelibrary.com). DOI: 10.1002/cnm.1385

Hemodynamic analysis of intracranial aneurysms with moving parent arteries: Basilar tip aneurysms

Daniel M. Sforza[1,*,†], Rainald Löhner[1], Christopher Putman[2] and Juan Raul Cebral[1]

[1]*Center for Computational Fluid Dynamics, Computational and Data Sciences Department, George Mason University, 4400 University Drive, MSN 6A2, Fairfax, VA 22030, U.S.A.*
[2]*Interventional Neuroradiology, Inova Fairfax Hospital, 3300 Gallows Road, Falls Church, VA 22042, U.S.A.*

SUMMARY

The effects of parent artery motion on the hemodynamics of basilar tip saccular aneurysms and its potential effect on aneurysm rupture were studied.

The aneurysm and parent artery motions in two patients were determined from cine loops of dynamic angiographies. The oscillatory motion amplitude was quantified by registering the frames. Patient-specific computational fluid dynamics (CFD) models of both aneurysms were constructed from 3D rotational angiography images. Two CFD calculations were performed for each patient, corresponding to static and moving models. The motion estimated from the dynamic images was used to move the surface grid points in the moving model. Visualizations from the simulations were compared for wall shear stress (WSS), velocity profiles, and streamlines.

In both patients, a rigid oscillation of the aneurysm and basilar artery in the anterio-posterior direction was observed and measured. The distribution of WSS was nearly identical between the models of each patient, as well as major intra-aneurysmal flow structures, inflow jets, and regions of impingement.

The motion observed in pulsating intracranial vasculature does not have a major impact on intra-aneurysmal hemodynamic variables. Parent artery motion is unlikely to be a risk factor for increased risk of aneurysmal rupture. Copyright © 2010 John Wiley & Sons, Ltd.

Received 15 September 2009; Revised 22 December 2009; Accepted 23 December 2009

KEY WORDS: cerebral aneurysms; hemodynamics; basilar artery; arterial wall motion; angiography

INTRODUCTION

The pathogenesis, progression and rupture of cerebral aneurysms are multi-factorial mechanisms that involve arterial hemodynamics, wall biomechanics, wall mechano-transduction or mechano-biology, and peri-aneurysmal environmental effects [1]. Although the relative importance and interaction of these factors is not entirely understood, hemodynamics is thought to play a fundamental role in these processes. Early studies of the hemodynamics in cerebral aneurysms were carried out on idealized geometries using both experimental [2] and computational models [3]. Subsequently, realistic experimental and computational models that replicate the patient-specific geometry have been created from medical images and analyzed using particle-image velocimetry and laser Doppler velocimetry [4], and computational fluid dynamics (CFD) [5–7] techniques.

*Correspondence to: Daniel M. Sforza, Center for Computational Fluid Dynamics, Computational and Data Sciences Department, George Mason University, 4400 University Drive, MSN 6A2, Fairfax, VA 22030, U.S.A.
†E-mail: dsforza@gmu.edu

Contract/grant sponsor: American Heart Association; contract/grant number: 0655413U
Contract/grant sponsor: Philips Medical Systems

These studies have identified variables of intra-aneurysmal hemodynamics that have been associated with previous aneurismal rupture including concentration of the inflow jet and impaction zone, and elevations in the maximum WSS [6].

As with all computational studies a number of assumptions are made to facilitate the computations. These assumptions are approximations or simplifications of the *in vitro* conditions that have the potential to impair the accuracy of the computational representation leading some to question whether the CFD can be relied on in the evaluation of aneurysm hemodynamics. Many of these assumptions have been studied to determine the relative sensitivity of small changes in the physiologic range on the CFD results. Because the majority of the previous studies have been performed under the assumption of rigid vessel walls and only a few studies included the radial pulsation of the arterial walls [8, 9], the effect of motion of the oscillation of the efferent and afferent arteries remains unknown.

The purpose of this work is to study the effect of arterial oscillation on the intra-aneurysmal hemodynamics by applying observed arterial oscillatory motions to our simulations. Specifically, the effects on the previously identified features, which have been associated with the history of previous rupture, will be analyzed in two basilar tip aneurysms. In these aneurysms, the motion of the arterial walls has been studied using dynamic imaging techniques based on multi-slice computed tomography angiography (4D CTA) and high frame rate X-ray digital subtraction angiography (DSA) [9, 10].

METHODS

Patients and images

Two patients with intracranial aneurysms imaged with dynamic DSA and 3D rotational angiography (3DRA) were selected from our database. Patient 1 was a 48 years old female with a 12.9 mm ruptured basilar tip aneurysm, whereas patient 2 was a 69 years old female with a 10.3 mm unruptured basilar tip aneurysm. These aneurysms were selected because they had the largest motion of the parent artery observed in a previous study of approximately 30 intracranial aneurysms [11]. Thus, the selected aneurysms represent the most extreme arterial wall motions observed *in vivo* using dynamic DSA. Both patients underwent conventional transfemoral catheterization and cerebral angiography using a Philips Integris Biplane angiography unit. Biplanar dynamic angiograms at 7.5 Hz were acquired during a 6-s contrast injection. In addition, an expert neuroradiologist (CP) measured the aneurysm maximum height and width on these projection views. This information was then used to establish the pixel size and to quantify the vascular wall excursion. The rotational angiography images were obtained during a 180° rotation and imaging at 15 frames/s for a total of 8 s. The corresponding 120 projection images were reconstructed into a 3D data set of $256 \times 256 \times 256$ voxels covering a field of view of 54.02 mm on a dedicated Phillips workstation. The imaging protocol was approved by the institutional review board and informed consent was obtained from all patients.

Arterial wall motion

The motion of the aneurysms and parent arteries were determined from cine loops of dynamic biplane angiography images as an oscillatory rotation on the median plane (there is no perceptible movement on the coronal plane). The amplitude and the center of the rotation were quantified using a manual rigid registration, as follows. All frames were examined to find the frames showing maximum displacement in the anterior/posterior directions. After these two frames were selected, both images were loaded in an image processing program as layers [12]. On each image, the contour of the aneurysm and the parent basilar artery were manually delineated using different colors. Then one image was made partially transparent and the two images were superposed. One of the images was rotated until the two delineations visually matched and the amplitude and the center of rotation were determined. The procedure was repeated to obtain a rough estimation of the error in the amplitude of the oscillatory motion. It was verified that the motion was well described

DOI: 10.1002/cnm

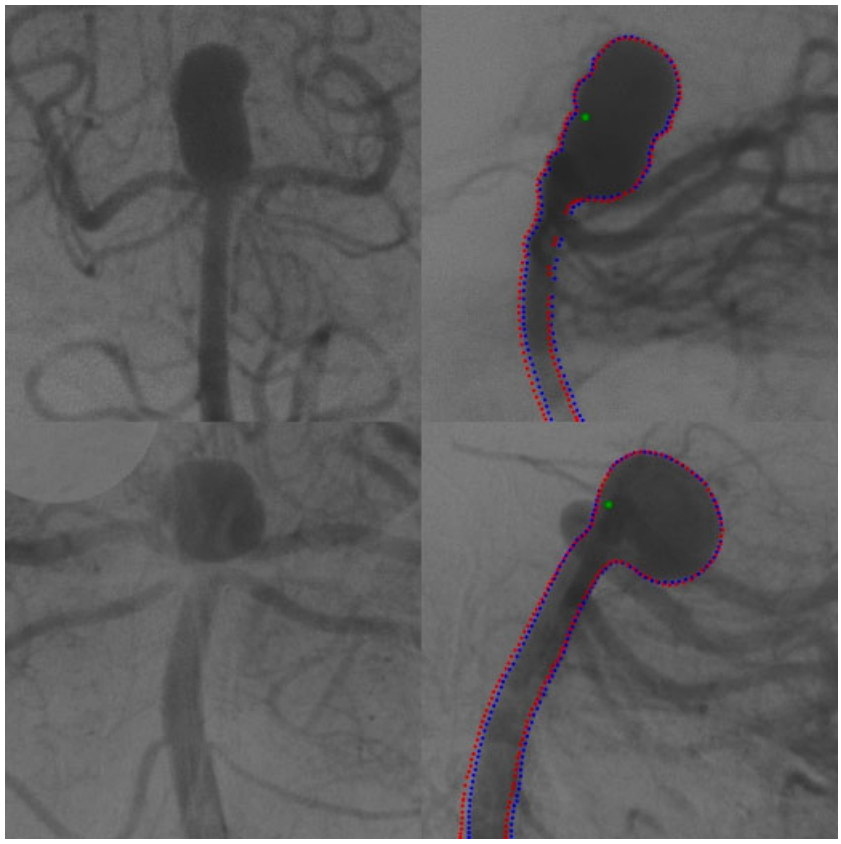

Figure 1. DSA images of both aneurysms in an anterior–posterior view (left column) and on the medial plane (right column). The vessel contours showing the maximum vessel wall displacements are shown on the medial planes. The dots inside the aneurysm indicate the location of the center of rotation of each aneurysm.

by a rigid rotation in the anterior–posterior plane by visually checking that the arterial delineations in different angiography frames coincided after rotating one of the images. Figure 1 shows DSA images of both aneurysms in an anterior–posterior view (left column) and on the medial plane (right column). The vessel contours showing the maximum vessel wall displacements are shown on the medial planes. The dots inside the aneurysm indicate the location of the center of rotation of each aneurysm.

Hemodynamics modeling

Patient-specific CFD models of the two aneurysms were constructed from the 3DRA images using a previously developed modeling pipeline [13]. Segmentation was performed with a seeded region growing algorithm to reconstruct the topology of the vascular network followed by an iso-surface deformable model to adjust the geometry to the vessel boundaries. The vascular model was then smoothed with a non-shrinking algorithm and vessels were truncated perpendicularly to their axis. Volumetric grids composed of tetrahedral elements were generated using an advancing front method with a resolution of 0.015 cm, resulting in approximately 2.6 and 1.0 million elements for patients 1 and 2, respectively. Previous studies have shown that this resolution is sufficient for clinically meaningful solutions [13–15]. Blood flow was considered as an incompressible Newtonian fluid (with density $\rho = 1.0\,\mathrm{g/cm^3}$ and viscosity $\mu = 0.04$ Poise) and was modeled by the unsteady Navier–Stokes equations in 3D. The diameters of the parent arteries of patients 1 and 2 were approximately 3 and 3.5 mm, and the Reynolds numbers based on these diameters varied from approximately 100 to 400. The governing equations were numerically solved using an implicit

DOI: 10.1002/cnm

arbitrary Lagrangian–Eulerian (ALE) finite element formulation on dynamic unstructured grids [16, 17]. The time-integration scheme can be written as a steady-state problem in pseudo-time τ:

$$v^{\theta}_{,\tau} + (v^{\theta} - w^{\theta}) \cdot \nabla v^{\theta} + \nabla p^{\theta} = \nabla \eta \nabla v^{\theta} - \frac{v^{\theta} - v^{n}}{\theta \Delta t} \tag{1}$$

$$\nabla \cdot v^{\theta} = 0 \tag{2}$$

where v is the velocity, w is the mesh velocity, p the pressure, η the kinematic viscosity, v^n denotes the velocity at the previous timestep and $v^{\theta} = (1-\theta)u^n + \theta u^{n+1}$. The parameter θ selects the numerical scheme: first-order implicit Euler scheme ($\theta = 1$), first-order explicit Euler scheme ($\theta = 0$), and second-order Crank–Nicholson scheme ($\theta = \frac{1}{2}$). These equations solved using a pressure-projection method and the spatial discretization is carried out using an edge-based upwind finite element method [18]. The discretized momentum equation is solved using a Generalized Minimal Residuals (GMRES) method and the discretized pressure Poisson equation is solved using a deflated preconditioned conjugate gradients method [19].

Since patient-specific flow conditions were not available, pulsatile physiologic flow rates derived from phase-contrast magnetic resonance measurements on normal subjects were prescribed at the inlet boundary using the fully developed Womersley profile [20, 21]. This is a reasonable approximation since the parent arteries did not have significant stenoses or evidence of other vascular diseases. The flow division from the parent artery to the outflow vessels was determined from their area ratio and the corresponding pressure boundary conditions were applied at the model outlets.

Two CFD calculations were performed for each of the two patients, corresponding to static and rigid oscillating models, respectively. The moving and static models of each aneurysm used the same computational grid, except that the grid point coordinates varied during the cardiac cycle in the moving models. The vascular wall motion observed in the dynamic DSA images was used to move the surface grid points. This was done by applying a time-dependent rigid rotation derived from the DSA images to the surface points. The interior mesh points were then updated using a non-linear velocity smoothing algorithm [17]. The basic idea of this algorithm is to solve an equation of the form

$$\nabla(k \cdot \nabla w) = 0 \tag{3}$$

where $k(d)$ is a function of the distance to the wall (d), and w is the mesh velocity. Since the velocity on the surface is known, Dirichlet boundary conditions are used to compute the mesh velocity at the interior mesh points:

$$w|_{\Gamma} = w_0 \tag{4}$$

with w_0 the surface mesh velocity. Subsequently, the mesh point coordinates are updated from

$$\frac{\mathrm{d}x}{\mathrm{d}t} = w \tag{5}$$

Since the dynamic DSA images were acquired with no cardiac gating or cardiac monitoring, there was no information available to synchronize the flow and wall motion waveforms. Therefore, it was first assumed that these waveforms were in phase, i.e. that the maximum wall displacement occurs at peak systole. Second, it was assumed that the maximum wall displacement occurs in the diastolic phase, which corresponds to a phase shift of about 20% between the corresponding waveforms. CFD simulations with moving walls under these two conditions were carried out.

A total of three cardiac cycles were computed using 100 timesteps per cycle, and it was verified that the results of the second and third cycles coincided. The results are therefore presented for the second cycle.

DOI: 10.1002/cnm

RESULTS

The motion of the basilar artery and the aneurysm observed in the DSA images of both patients could be well represented by an oscillatory rigid rotation around a center of rotation located close to the basilar tip in the medial plane near the anterior wall of the aneurysm and midway between the neck and the fundus of the aneurysm. No motion was observed in the perpendicular (anterior–posterior) view. The amplitude and time dependence were similar on both patients. The amplitude of the rotational motions were $1.16 \pm 0.16°$ and $1.11 \pm 0.12°$ for patients 1 and 2, respectively.

Visualizations of the velocity fields, flow patterns, and wall shear stress (WSS) distributions at peak systole for the static and oscillating models are presented in Figures 2 and 3 for patients 1 and 2, respectively. These figures show velocity contours on the medial plane (top left) and on a plane through the aneurysm neck (top right), streamlines (bottom left), and WSS contours on the aneurysm surface (bottom right). The blue lines correspond to the static models, whereas the red lines correspond to the oscillating models. These visualizations show that although the motion of the basilar arteries were among the largest observed in a series of intracranial aneurysms imaged with dynamic DSA, little differences in the velocity fields and WSS distributions can be observed between the static and the moving models. Therefore, the hemodynamics of the static and the moving models is qualitatively in very good agreement for both patients. Adding a 20% phase shift between the flow and the wall motion waveforms did not substantially modify these results.

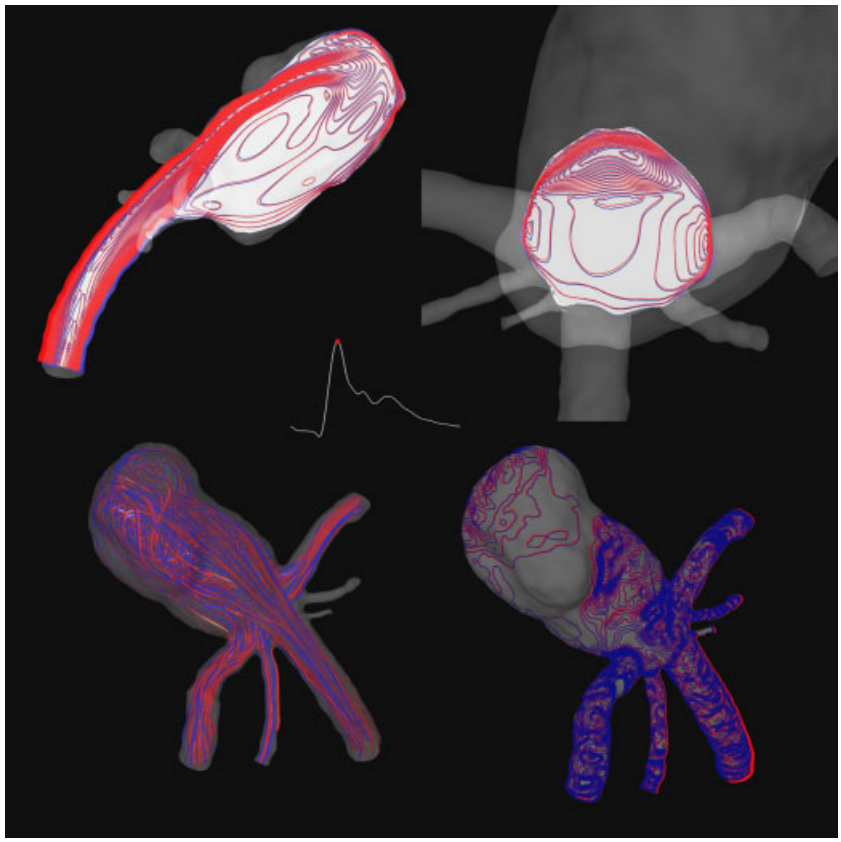

Figure 2. Visualizations of the velocity and wall shear stress fields at peak systole for patient 1 using the static (blue) and moving (red) models. Top: 30 velocity contours in the range [0–100] cm/s on a coronal plane (left) and on a plane through the aneurysm neck (right). Bottom: streamlines (left) and 30 wall shear stress contours in the range [0–300] dyne/cm^2.

DOI: 10.1002/cnm

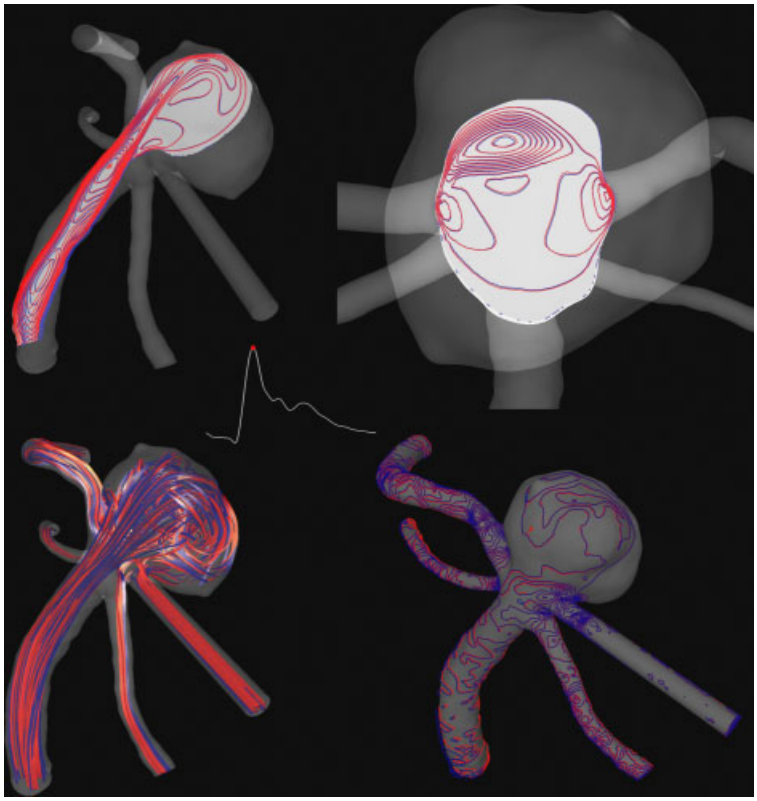

Figure 3. Visualizations of the velocity and wall shear stress fields at peak systole for patient 2 using the static (blue) and moving (red) models. Top: 20 velocity contours in the range [0–77] cm/s on a coronal plane (left) and on a plane through the aneurysm neck (right). Bottom: streamlines (left) and 30 wall shear stress contours in the range [0–300] dyne/cm^2.

Graphs of the WSS magnitudes obtained with both models for each patient are presented in Figure 4 (top row). In these plots, the x-axis corresponds to the WSS computed by the static model and the y-axis the WSS computed with the moving model, at the same grid points. It can be clearly seen that both models are in close agreement, for both patients. The relative difference in the local values of the WSS magnitude between the static and the moving models is below 5%. Linear regressions of the WSS values obtained with the static and the moving models of each aneurysm indicate no relative over or under estimation of the WSS magnitude between these models (slopes values were 0.9912 and 0.9990 for patients 1 and 2, with $R^2 = 0.999918$ and 0.999947, respectively). The corresponding visualizations of the distributions of WSS magnitudes at peak systole for both patients are also presented in Figure 4 (bottom row).

DISCUSSION

Computational approaches to the study of cerebral aneurysms and the interaction with the intra-aneurysmal hemodynamics have yielded several interesting associations that influence our thinking about the mechanisms responsible for aneurysm formation, growth, and ultimate rupture. Cebral *et al.* [6] showed using patient-specific models that aneurysms with a previous history of rupture were associated with focus inflow jets, small impaction zones, and complex intra-aneurysmal flow patterns. Other studies have pointed to either elevation or depression of WSS measures in ruptured aneurysms [7, 22].

DOI: 10.1002/cnm

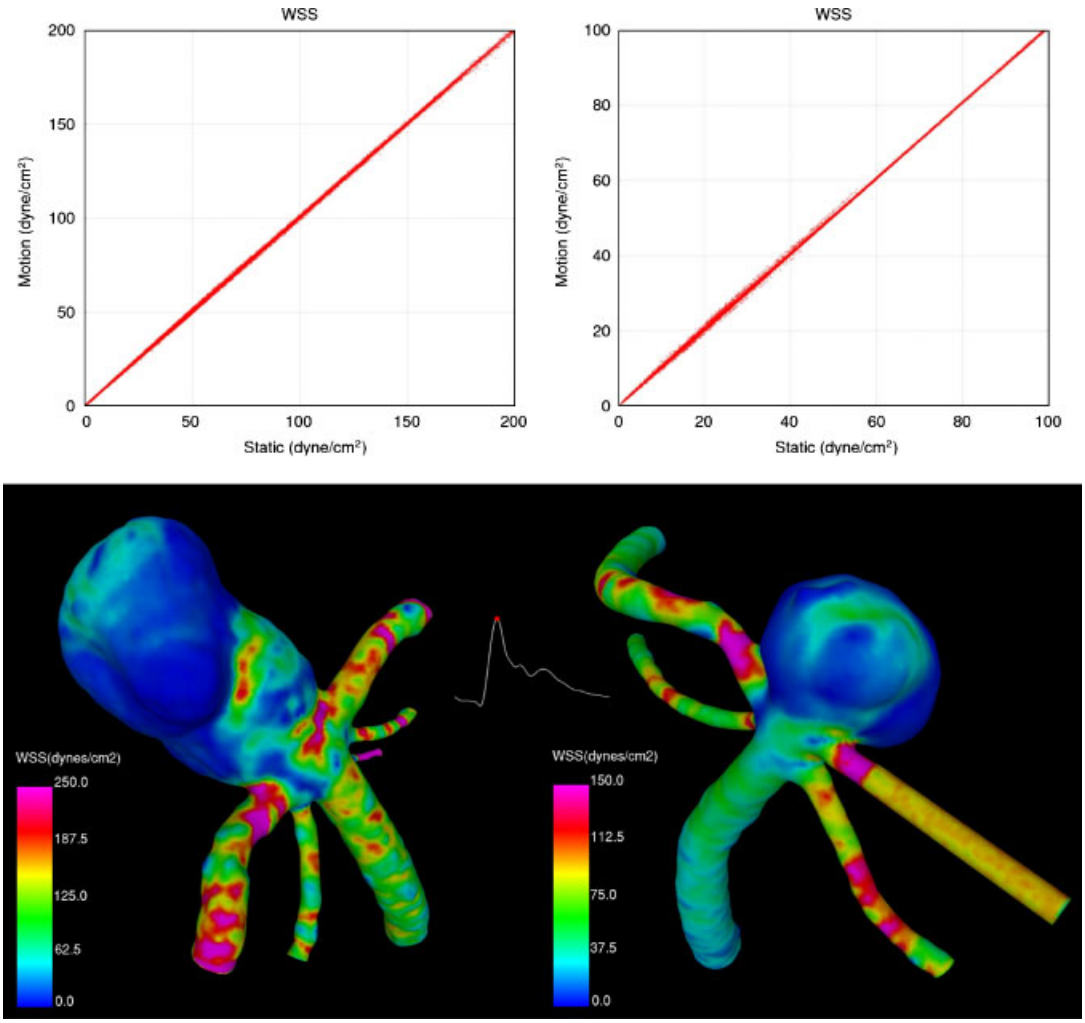

Figure 4. Top: graphs of the WSS computed by the static model (x-axis) vs the WSS computed with the moving model (y-axis) for patients 1 (left) and 2 (right). Bottom: visualizations of the WSS magnitude distributions at peak systole for patients 1 (left) and 2 (right).

All previous works using computational techniques have in common the use of assumptions that are approximations of the *in vitro* conditions. Typically, CFD simulations use a simplification of the conditions because of either a lack of specific information regarding the condition or as a means of simplifying or facilitating the computations. Implicitly, the investigator is making a judgment that the assumptions are close enough to the *in vitro* condition that they will not significantly affect the computation result.

In the study of aneurismal pathophysiology in relation to intra-aneurysmal hemodynamics, the investigator has a difficult problem. In order to determine whether an assumption is appropriate, the investigator must know what outcome parameters are important. Because methods of measurement of intra-aneurysmal flow conditions are just now being developed, the investigator has to rely largely on computational methods. Now that the important parameters that affect aneurismal pathophysiology are becoming known. It is critical that the assumptions be carefully tested so that any distortions of the CFD results can be minimized and understood.

Previous works have studied different aspects of basilar aneurysms using CFD, such as how flow patterns are influenced by the parent-artery angle [23, 24] and surgical intervention [25], and comparison of CFD results to *in vivo* MRI measurements [26]. Furthermore, the motion of arterial

DOI: 10.1002/cnm

and aneurysms walls have been observed, described, and simulated [9–11, 27], but to the best knowledge of the authors this is the first work to simulate the observed motion of the parent artery.

We have observed using dynamic high frame rate angiography that the basilar artery has a small motion that could be well represented by an oscillatory rigid rotation around a center of rotation located close to the basilar tip in the medial plane near the anterior wall of the aneurysm and midway between the neck and the fundus of the aneurysm. *A priori* one could think that the observed arterial motion could concentrate, spread, or deviate the aneurysm inflow jets, or substantially change the flow impaction zones or regions of low or elevated WSS, and therefore could be a major factor in the rupture risk assessment of aneurysms at this location. However, this study suggests that the motion of the parent artery has little effect on the aneurysm hemodynamics. The effect is likely minimized by only small displacement of the artery as well as the rigidity of the rotation. This apparently rigid displacement maintains the relative angles of the arteries and the aneurysm and consequently minimizes the effect. Finally, the velocity of the arterial wall in the displacement is very small when compared with the velocity of the blood flow. Hence, distortion of the developed flow stream is minimal.

This study does not address other potential effects of parent artery motions. Parent artery motion could still have an important effect on the arterial wall stresses and/or accentuate the interactions between the aneurysm and the surrounding environment. These questions will require more detailed study.

The current study has other limitations that should be considered when assessing the results of this work. The accuracy of the wall motion estimation from dynamic DSA images is limited by the image spatial and temporal resolution. The aneurysms selected for this study were among the ones with the largest parent artery motions observed. In these cases, the wall displacement is substantially larger than the image resolution. The motion of the parent artery was approximated as a rigid rotation of the medial plane around a point near the basilar tip. No pulsatile motion of the vessel wall was included. The motion of the vessel wall observed in the dynamic DSA images could be well represented by this rigid rotation with no pulsation. Previous studies of the influence of pulsatile motion of the vessel wall on aneurysmal hemodynamics suggested that rigid models could slightly overestimate the WSS with respect to pulsating models [9]. No patient-specific flow conditions were available. Nevertheless, the static and the moving wall models were in very close agreement during the entire cardiac cycle. In the moving wall models, the vessel wall displacement was synchronized with the peak of the pulsatile flow waveform used as the inflow condition. Adding a phase difference of about 20% between the flow and the displacement waveforms did not substantially alter the results. Only two aneurysms were included in this study. Although the motions of the basilar arteries of these patients were quite large, the conclusion of no change in the hemodynamics cannot be generalized to the entire population. This result should have to be tested with a larger sample. Despite these limitations, these models can help us to better understand the influence and the importance of the motion of the parent artery on the intra-aneurysmal hemodynamics.

CONCLUSIONS

Although the basilar artery can exhibit a significant oscillatory motion, it has little effect on the hemodynamics of basilar tip aneurysms. Thus, CFD models with a static proximal artery provide a good approximation of the *in vivo* hemodynamic conditions in aneurysms at this location. Studies of aneurysm pathophysiology using image-based CFD methods to represent the intra-aneurysmal flow characteristics and WSS distributions can be carried out without incorporating the parent artery oscillatory motion.

ACKNOWLEDGEMENTS

We thank the American Heart Association (Grant #0655413U) and Philips Medical Systems for financial support.

DOI: 10.1002/cnm

REFERENCES

1. Sforza D, Putman CM, Cebral JR. Hemodynamics of cerebral aneurysms. *Annual Review of Fluid Mechanics* 2009; **41**:91–107.
2. Liou TM, Liou SN. A review of in vitro studies of hemodynamic characteristics in terminal and lateral aneurysm models. *National Scientific Council ROC* (*B*) 1999; **23**:133–148.
3. Burleson AC, Strother CM, Turitto VT. Computer modeling of intracranial saccular and lateral aneurysms for the study of their hemodynamics. *Neurosurgery* 1995; **37**:774–784.
4. Tateshima S, Murayama Y, Villablanca JP *et al.* In vitro measurement of fluid-induced wall shear stress in unruptured cerebral aneurysms harboring blebs. *Stroke* 2003; **34**:187–192.
5. Steinman DA, Milner JS, Norley CJ, Lownie SP, Holdworth DW. Image-based computational simulation of flow dynamics in a giant intracranial aneurysm. *AJNR American Journal Neuroradiology* 2003; **24**:559–566.
6. Cebral JR, Castro MA, Burgess JE, Pergolizzi R, Sheridan MJ, Putman CM. Characterization of cerebral aneurysm for assessing risk of rupture using patient-specific computational hemodynamics models. *AJNR American Journal of Neuroradiology* 2005; **26**:2550–2559.
7. Shojima M, Oshima M, Takagi K *et al.* Magnitude and role of wall shear stress on cerebral aneurysm: computational fluid dynamic study of 20 middle cerebral artery aneurysms. *Stroke* 2004; **35**:2500–2505.
8. Valencia A, Solis F. Blood flow dynamics and arterial wall interaction in a saccular aneurysm model of the basilar artery. *Computers and Structures* 2006; **84**:1326–1337.
9. Dempere-Marco L, Oubel E, Castro MA, Putman CM, Frangi AF, Cebral JR. *Estimation of Wall Motion in Intracranial Aneurysms and its Effects on Hemodynamic Patterns*. Lecture Notes in Computer Science, vol. 4191. Springer: Berlin, 2006; 438–445.
10. Ishida F, Ogawa H, Simizu T, Kojima T, Taki W. Visualizing the dynamics of cerebral aneurysms with four-dimensional computed tomography angiography. *Neurosurgery* 2005; **57**:460–471.
11. Sforza D, Putman CM, Oubel E, DeCraene M, Frangi AF, Cebral JR. Characterization of cerebral aneurysm wall motion from dynamic angiography. *American Journal of Neuroradiology* 2009; submitted.
12. GIMP: GNU Image Manipulation Program. Available from: www.gimp.org.
13. Cebral JR, Castro MA, Appanaboyina S, Putman CM, Millan D, Frangi AF. Efficient pipeline for image-based patient-specific analysis of cerebral aneurysm hemodynamics: technique and sensitivity. *IEEE TMI* 2005; **24**:457–467.
14. Löhner R, Appanaboyina S, Cebral JR. Parabolic recovery of boundary gradients. *Communications in Numerical Methods in Engineering* 2007; **24**:1611–1615.
15. Radaelli A, Ausburger L, Cebral JR *et al.* Reproducibility of haemodynamical simulations in a subject-specific stented aneurysm model—a report on the Virtual Intracranial Stenting Challenge 2007. *Journal of Biomechanics* 2008; **41**:2069–2081.
16. Cebral JR, Yim PJ, Löhner R, Soto O, Choyke PL. Blood flow modeling in carotid arteries using computational fluid dynamics and magnetic resonance imaging. *Academic Radiology* 2002; **9**:1286–1299.
17. Löhner R, Yang C, Cebral JR *et al.* Fluid–structure–thermal interaction using adaptive unstructured grids. In *Computational Methods for Fluid–Structure Interaction,* Kvamsdal (ed.). Tapir Press: Norway, 1999; 109–120.
18. Löhner R. *Applied CFD Techniques*. Wiley: New York, 2001.
19. Mut F, Aubry R, Löhner R, Cebral JR. Fast numerical solutions in patient-specific simulations of arterial models. *Communications in Numerical Methods in Engineering*, 2009; DOI: 10.1002/cnm.1235.
20. Womersley JR. Method for the calculation of velocity, rate of flow and viscous drag in arteries when the pressure gradient is known. *Journal of Physiology* 1955; **127**:553–563.
21. Cebral JR, Castro MA, Putman CM, Alperin N. Flow–area relationship in internal carotid and vertebral arteries. *Physiological Measurement* 2008; **29**:585–594.
22. Castro MA, Putman CM, Radaelli A, Frangi AF, Cebral JR. Hemodynamics and rupture of terminal cerebral aneurysms. *Academic Radiology* 2009; **16**:1201–1207.
23. Ford MD, Lee S-W, Lownie SP, Holdsworth DW, Steinman DA. On the effect of parent-aneurysm angle on flow patterns in basilar tip aneurysms: towards a surrogate geometric marker of intra-aneurismal hemodynamics. *Journal of Biomechanics* 2008; **41**:241–248.
24. Valencia AA, Guzman AM, Finol EA, Amon CH. Blood flow dynamics in saccular aneurysm models of the basilar artery. *Journal of Biomechanical Engineering* 2006; **128**:516–526.
25. Rayz VL, Lawton MT, Martin AJ, Young WL, Saloner D. Numerical simulation of pre- and postsurgical flow in a giant basilar aneurysm. *Journal of Biomechanical Engineering* 2008; **130**:021004–021006.
26. Rayz VL, Boussel L, Acevedo-Bolton G *et al.* Numerical simulations of flow in cerebral aneurysms: comparison of CFD results and in vivo MRI measurements. *Journal of Biomechanical Engineering* 2008; **130**:051011–051019.
27. Perktold K, Peter R, Resch M. Pulsatile non-Newtonian blood flow simulation through a bifurcation with an aneurysm. *Biorheology* 1989; **26**:1011.

DOI: 10.1002/cnm